

Rapid One Step Fabrication of Hydrophilic Hierarchical Porous PDMS with Negative Piezopermittivity for Sensing and Energy Storage Applications

Chithra Parameswaran, Raghvendra Pratap Chaudhary, Sagar Hosangadi Prutvi, and Dipti Gupta*



Cite This: *ACS Appl. Polym. Mater.* 2022, 4, 2047–2056



Read Online

ACCESS |

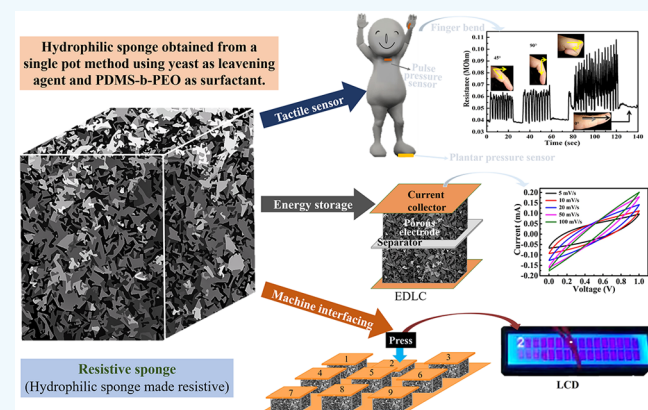
Metrics & More

Article Recommendations

Supporting Information

ABSTRACT: A simple, cost-effective, scalable, one step synthesis method for obtaining a hydrophilic poly(dimethylsiloxane) (PDMS) sponge using an effervescence template and surfactant is provided here. The porosity of the sponge can be tuned ($\sim 25\%$ to $\sim 60\%$) by varying the yeast concentration, volume, and curing temperature. A confined dispersion for standard deviation of pore parameters from statistical analysis shows good repeatability, homogeneity, and convergence of sponge porosity and pore area. A contact angle study shows the hydrophilic nature of the obtained sponge with the introduction of the surfactant. Fourier transform infrared spectroscopy (FTIR) confirms the single-step process with the absence of alive yeast cell constituents with the synergistic effect of PDMS backbone and hydrophilic moieties alone. In-situ tomography compression study shows little deviation ($\sim 4\%$) in pore structure for before and after load applied conditions of sponge with good resilience. The sponge exhibits negative piezopermittivity with applied pressure due to the densification of pores leading to dipole cancellation. The bare sponge is applied to capacitive sensing for large pressure range sensing (sensitivity $\sim 0.03\text{ kPa}^{-1}$, $< 45\text{ kPa}$) and modified as a resistive pressure sensor (sensitivity $\sim 0.3\text{ kPa}^{-1}$, $< 10\text{ kPa}$; $\sim 0.02\text{ kPa}^{-1}$, $< 50\text{ kPa}$), to human-machine interfacing, and as supercapacitor ($\sim 11.43\text{ mF/g}$) electrode.

KEYWORDS: hydrophilic elastomer sponge, effervescence template, single pot fabrication, negative piezopermittivity, pressure/strain sensor, porous electrode, human-machine interface, supercapacitor



1. INTRODUCTION

Elastomer sponges are of profound interest and are applied to large number of applications like biosensing,^{1–10} water purification,^{11–14} energy storage,^{15,16} photocatalysis,¹⁷ microfluidic pump systems,^{18–20} subcutaneous and intraperitoneal applications,²¹ and so on as they possess exceptional properties such as being lightweight, compressible,^{22,23} resilient,²⁴ composition tunable,²⁵ and biodegradable.^{26–28} The morphology of these sponges have a 3D strut structure interconnected through smaller pores as hierarchical features in either open-cell or closed-cell forms. These three-dimensional structure are imparted to the elastomer by many multistep processes.^{29,10}

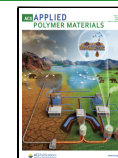
Elastomer sponges are inherently hydrophobic; however, hydrophilic sponges find wider applications albeit their tedious processes. Conventional methods of obtaining hydrophilic surface are plasma treatment (which requires vacuum systems, is costly, is time-consuming, and has a low shelf life) and functionalizing using surfactant (hydrophilicity can be retained for a relatively longer time).^{18,30–33} These porous elastomers are widely used in sensors that take either capacitive, resistive or piezoelectric configurations, with porous structure imparting

them with cyclic stability, long-range pressure sensing, sensitivity, and replicable performance.^{2,15,34,35} Elastomer sponge based sensors are the low-cost alternative to other sensing platforms. However, these are encountered with a few limitations: (i) the pressure range achievable for sensing is limited to approximately a few kPa, (ii) the fabrication process is tedious including multi-step processes with little control on porosity, and (iii) the obtained sponge cannot be functionalized with a longer shelf life for resistive mode sensing. In this context, a method of obtaining hydrophilic elastomer sponge is essential that can be implemented for large pressure sensing in both capacitive and resistive modes. Low-cost approaches are

Received: December 25, 2021

Accepted: January 24, 2022

Published: February 4, 2022



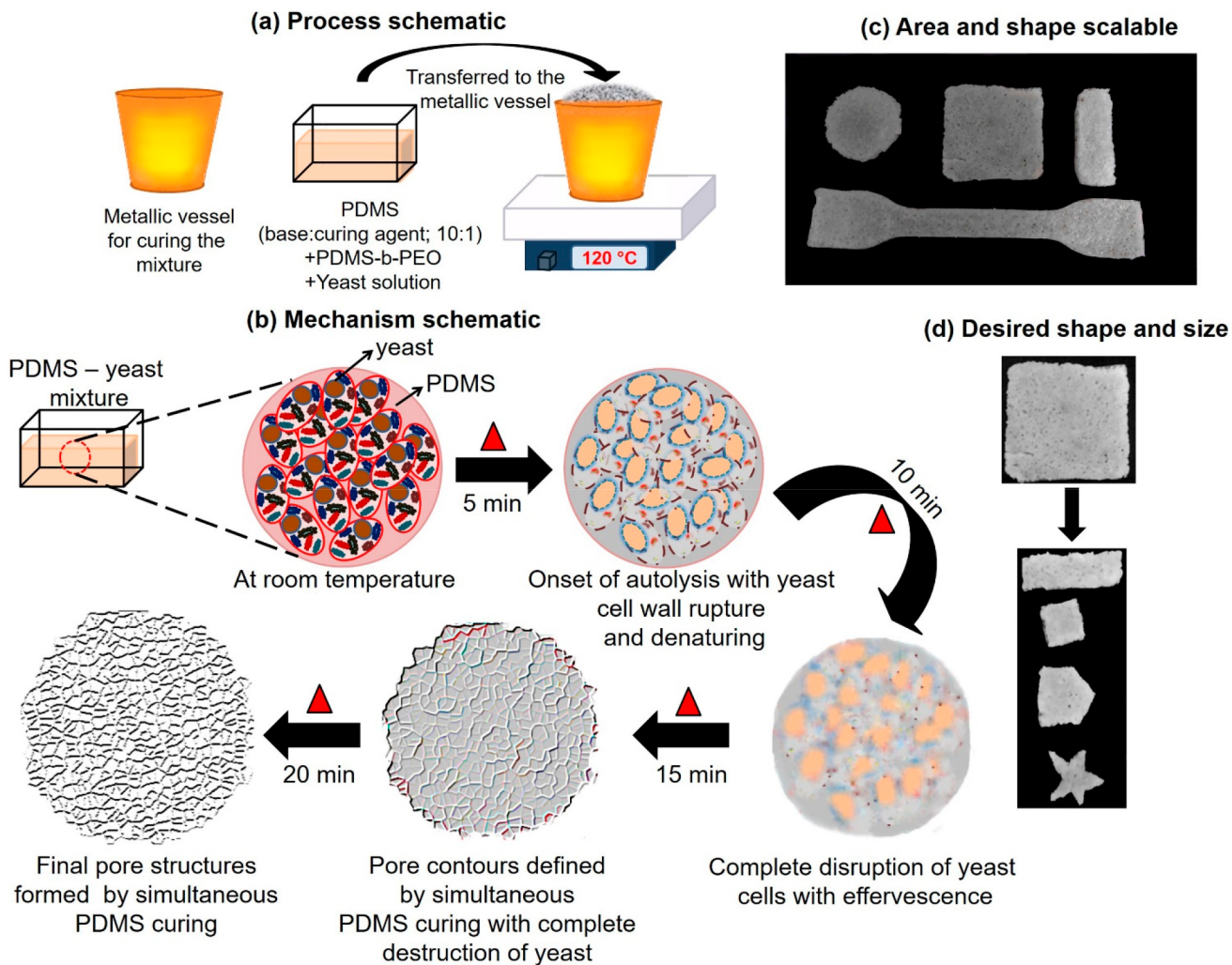


Figure 1. (a) Process schematic of sponge fabrication. (b) Schematic of mechanism involved in the formation of 3D hydrophilic sponge. (c, d) Large area and desired shape molded sponge.

targeted at that can produce at par performance with existing technology.³⁶

Here, we introduce autolysis of yeast in conjunction with poly(dimethylsiloxane-*b*-ethylene oxide) (PDMS-*b*-PEO) as a surfactant for hydrophilic PDMS sponge fabrication. The compatibility of surfactant with PDMS, the uniform dispersion of yeast solution, and the availability of hydrophilic group throughout the volume facilitate complete volume hydrophilicity in the sponge. The effects of yeast concentration and volume on the pore size and porosity are discussed, highlighting their distribution over several trials to confirm the repeatability of the approach. The effect of curing temperature on the sensing activity of the resistive pressure sensor devised from it provides tuning of sensitivity through porosity. A detailed study of the material aspect is carried out to identify the effect of material property attributed to the sensing action of the sponge in both the capacitive and resistive modes of operation. The resistive sponge is also then implemented in real-time display of a number pad, as proof of concept for a human–machine interface and as a supercapacitor electrode.

2. EXPERIMENTAL DETAILS

2.1. Materials. Yeast was purchased from Crown from a local supermarket. PDMS was procured from Dow Corning (Sylgard 184) as a two-part kit, PDMS-*b*-PEO from Polysciences, and the conductive ink from Bare Conductive (Bare Conductive Ltd.). All the materials were used as received without further purification. Deionized (DI) water was used for all experiments.

2.2. Experimental Procedure. Initially, the yeast is proofed for its activity. For this, a small quantity of yeast is soaked in DI water and kept idle for ~5 min. The formation of froth confirms its activity. It is then sonicated for 1 min to blend into a uniform solution and is used immediately in the fabrication of PDMS sponge or it can be refrigerated for later use. PDMS resin and 4 wt % surfactant are weighed, and yeast solution is added to it dropwise and mixed thoroughly. It is then transferred to a metallic vessel and heated for 20 min to obtain the final hydrophilic PDMS sponge (Figure 1a). The sponge is then washed under running DI water and dried in air.

2.3. Characterization Techniques. Morphology was studied using a scanning electron microscope (ESEM200; FEI Quanta). Sponge profile data like pore size and porosity were extracted from the morphology study using the particle analyzer utility in ImageJ software. Statistical analysis was carried out on the extracted pore data. In situ compression morphology studies were performed using a Four Dimension X-ray microscope (FDXM, Xradia Versa 520: Zeiss). Fourier transform infrared spectroscopy (FTIR, 3000 Hyperion Microscope with Vertex 80 FTIR System, Bruker, Germany) has been

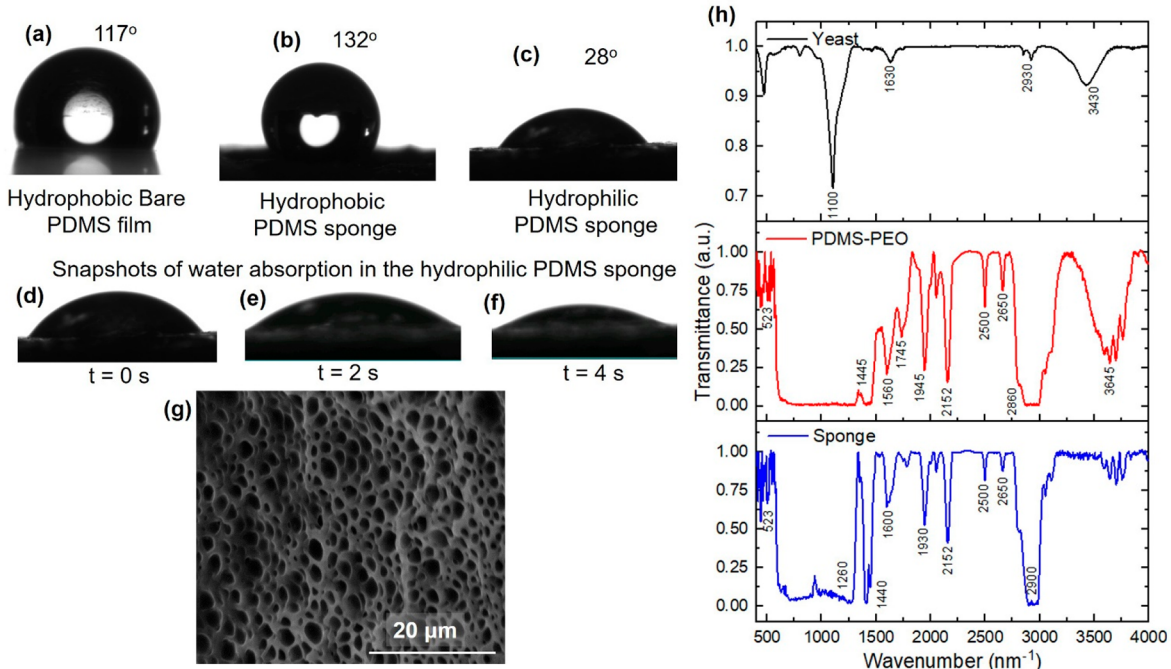


Figure 2. (a–c) Contact angle comparison showing the hydrophilic nature of the sponge. (d–f) Absorption of the water droplet into the sponge volume showing complete volume hydrophilicity. (g) Electron microscope image of final optimized porous morphology. (h) FTIR spectra comparison showing complete removal of live yeast.

used for chemical composition analysis. The hydrophilicity of the complete sponge was confirmed from contact angle measurement (Dataphysics OCA 15). Dielectric properties were extracted using a Broadband dielectric spectrometer over a frequency range of 0 Hz to 10 MHz (Novocontrol Technologies, Germany, Concept 80). Electromechanical performance was recorded and studied using a universal tensile machine (MARK 10, ESM 303) and an Agilent U1732a hand-held LCR meter for capacitive sensor and a Keysight 4200 for the resistive sensor. Electrochemical characterization was carried out in Autolab (PGSTAT 101) for the supercapacitor electrode performance study.

3. RESULTS AND DISCUSSION

3.1. Fabrication and Composition Analysis of Hydrophilic Sponge. Yeast (*Saccharomyces cerevisiae*, a eukaryotic single cellular organism) undergoes plasma membrane permeabilization and ion leakage into the cytoplasm followed by cell death when subjected to a sudden temperature rise above its physiological limit (25–50 °C). The cell walls constituted of glucans are insoluble in water and are released into the medium during plasma membrane lysis. The bilayer cell wall ($\beta \rightarrow 1, 3$ glucans forming the inner cell wall and its complex with chitin forming the outer cell wall, which is linked by $\beta \rightarrow 1, 6$ glucan fibrous structures) undergoes permeabilization preceding cell death.^{36–39} This temperature-dependent autolysis of the yeast with effervescence and simultaneous curing of PDMS yields the elastomer sponge (Figure 1). As shown in Figure 1b, after heating of the sample for ~5 min, cell wall rupture marks the onset of autolysis, which, when further subjected to prolonged heating, initiates effervescence. The temperature being nominal for the resin curing, simultaneous curing of PDMS traps the effervescence taking the shape of these air bubbles. Upon further heating, complete pore formation and evaporation of water in the mixture marks the culmination of the process. The area and shape of the sponge can be defined by the choice of vessel used

for curing (Figure 1c). The bigger sponge can also be easily cut into smaller pieces as the sponge is soft (Figure 1d).

The hydrophilicity and chemical composition (Figure 2) are studied from contact angle measurement and FTIR spectroscopy, respectively. Figure 2a–c elaborates on the hydrophilic nature of the sponge with the contact angle measured at the surface for droplets of water suspended over it. A decrease in contact angle from 132° to 28° shows explicit transformation from hydrophobic to hydrophilic nature. Figure 2d–f shows the absorption of water drop into the sponge volume captured at every 2 s with the drop meniscus decreasing upon absorption into the interior of the sponge volume. This volume hydrophilicity is observed as a two-step process. Initially, the water droplet wets the surface (base circle radius increases over time), and then it is absorbed into the inner layer of sponge (drop height, as well as base circle radius, decreases over time), unlike a hydrophilic surface where the wetting continues indefinitely with an increase in the base circle alone. This contact angle measurement depicts complete volume hydrophilicity of our sponge in contrast to either the temporary or subsurface hydrophilicity reported.^{31,40–42} Figure 2g shows the SEM image of fine homogeneous porous features. The single pot synthesis of hydrophilic elastomer sponge is validated with the help of FTIR spectroscopy. Comparing the FTIR responses of the final sponge with the individual precursors (Figure 2h) substantiates the single-step method proposed here. The absence of signature peaks of live yeast in the sponge confirms the complete dissociation of it, giving a single pot fabrication.

Table 1 shows the significant peaks present in the final hydrophilic sponge inherited from both yeast and the siloxane components.

Thus, the yeast plays a sacrificial role of effervescence creation with complete dissociation through its temperature mediated autolysis, creating a volume hydrophilic elastomer

Table 1. Compositional Analysis of Sponge Revealing the Sacrificial Role of Yeast

wavenumber (cm ⁻¹)	composition
501	Si—O—Si stretch vibrations ⁴³
792	CH ₃ asymmetric rocking and Si—C asymmetric stretching ⁴³
847	Si—H wagging ⁴³
1015	Si—O—Si symmetric stretching ⁴³
1039	Mannan band (C—O—C, C—C, C—OH stretching of pyranose ring) ⁴⁴
1075	Si—O—Si asymmetric stretching ⁴³
1076	$\beta(1 \rightarrow 3)$ glucan band (C—O—C, C—C, C—OH stretch of pyranose ring and O—P—O, C—O—P stretching) ⁴⁴
1260	symmetric bending vibrations of CH ₃
1545	Amide II: N—H, C—N vibrations of the peptide bond in different protein conformations ⁴⁶
1650	Amide I: C=O vibrations of different protein structures ⁴⁶

sponge. This volume hydrophilicity, achieved through a single pot synthesis technique, makes our process facile, rapid, and frugal.

3.2. Porosity Variation with Yeast Solution Concentration. A study on the concentration of yeast on the pore morphology (Figure 3) was carried out to understand the feasibility on porosity control. Yeast solutions of concentrations of 0.1 to 0.5 g in 3 mL of DI water were prepared. A systematic progression of pore formation with initial contour

definition and further blooming into complete open pores with increase in yeast concentration is observed here (Figure 3a–e). At low yeast concentrations, the effervescence formed is insufficient to sustain until complete curing of PDMS leading to the closing of the pores giving little or no pores. Thus, only pore contours are formed. At higher concentrations, the effervescence formed sustains for longer duration giving half-formed porous features. As the concentration is further increased, the autolysis produces sufficient effervescence that can sustain until complete curing of the PDMS giving well-defined pores. This attributes to the formation of pores which is dependent on gas evolution that can sustain until complete curing of PDMS. Thus, the need for optimum yeast concentration for a fixed quantity of PDMS is validated from this study. The porosity increases from 30% to 60% with an increase in yeast concentration from 0.1 to 0.5 g in 3 mL of DI water (Figure 3f). The pore size increases initially and decreases with an increase in yeast concentration (Figure 3g). This is because the denser effervescence present in the mixture gives rise to more air traps leading to smaller size within the constrained mixture volume. The standard deviation of porosity (Figure 3f) and pore size (Figure 3g) has a confined dispersion about their mean values which illustrate good repeatability and homogeneity over several trials.

3.3. Porosity Control with Volume of Yeast Solution. The optimized concentration of 0.5 g/3 mL from the above

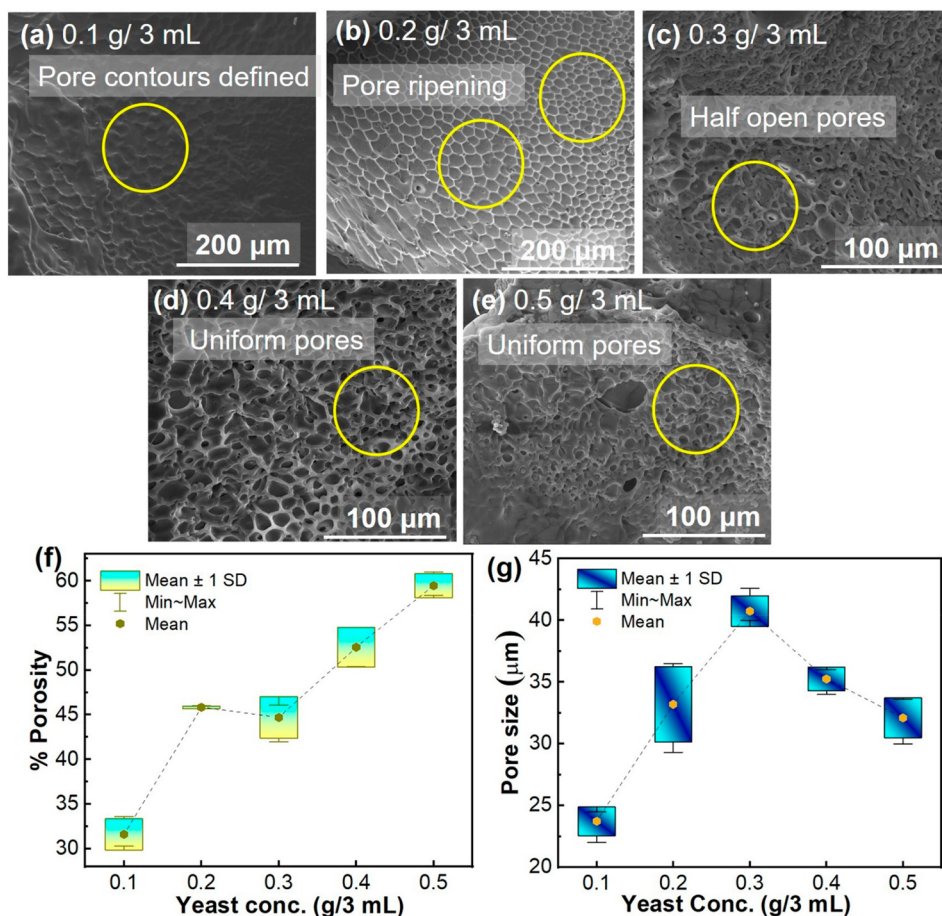


Figure 3. (a–e) Electron microscope images of the porous structure of sponge obtained for varied concentration of yeast solution from 0.1 to 0.5 g in 3 mL of DI water in steps of 0.1 g in 3 mL of DI water, respectively. (f) Percent porosity variation and (g) pore size variation with increase in yeast concentration in the sponge.

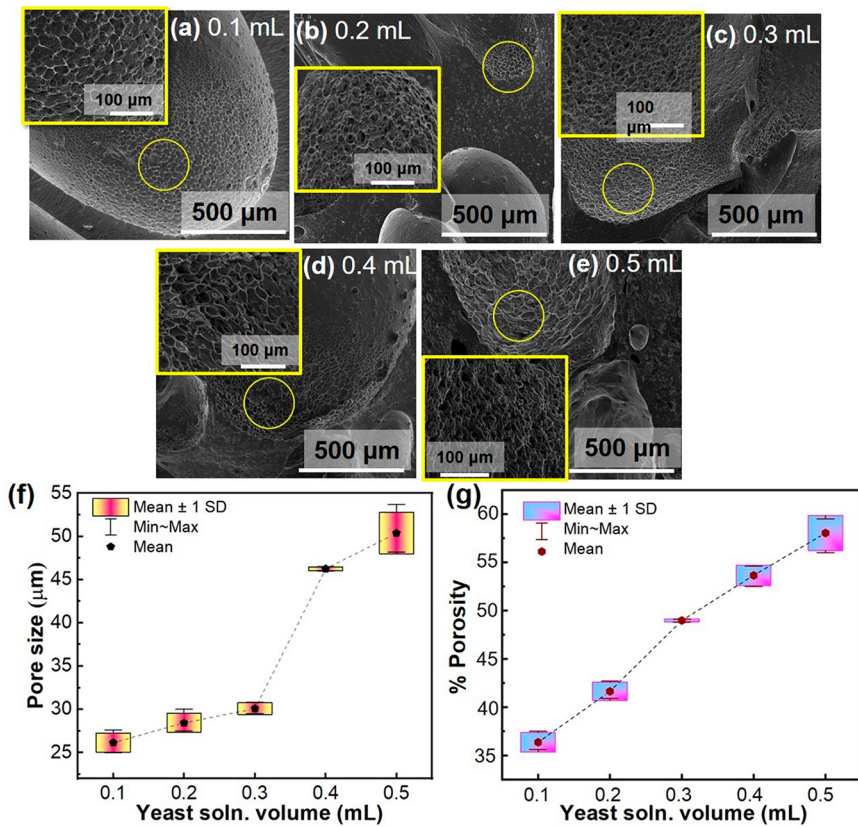


Figure 4. (a–e) SEM images of sponge showing effect of yeast volume on pore formation and porosity. (f) Variation of pore size and (g) variation of percent porosity with yeast volume.

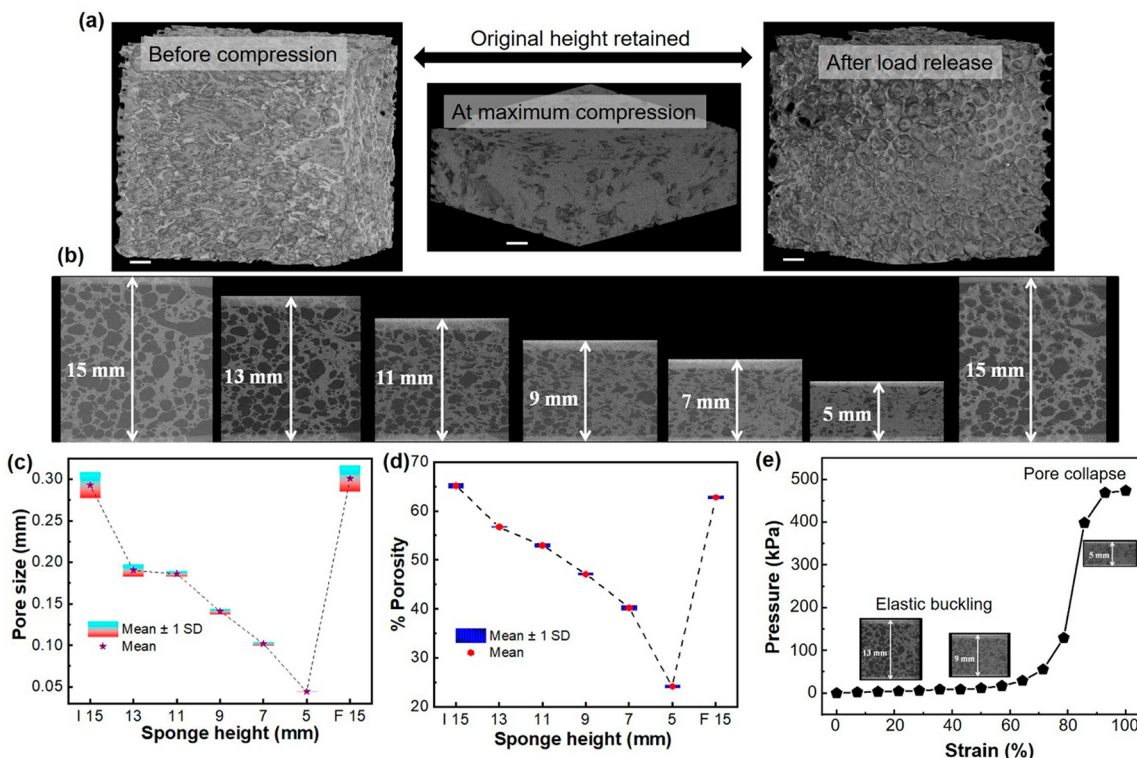


Figure 5. (a) Tomography of sponge at stages of no load, at complete compression, and after load removal. Scale bar reads 1 cm. (b) Cross section at each stage of successive compression at different heights of compression. (c) Variation in average pore size and (d) variation of percent porosity at different stages of applied stress. I15 denotes the initial condition and F15 denotes the final condition after load is removed. (e) Stress–strain curve showing elastic buckling and pore collapse regions.

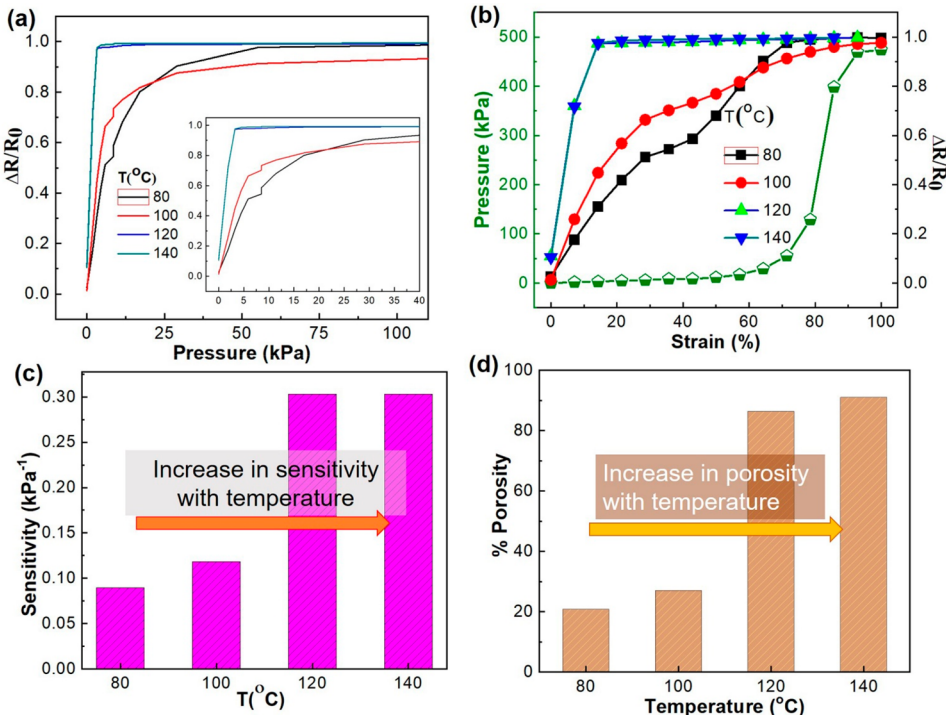


Figure 6. (a) Relative resistance vs pressure (inset shows the low pressure range). (b) Relative resistance vs strain. (c) Sensitivity curves for applied pressure. (d) Percent porosity variation of the different samples at no load condition.

study was varied in volume from 0.1 to 0.5 mL for 3 g of a PDMS mixture to study the effect of yeast solution volume on porosity and pore size (Figure 4). Crude pores are obtained for fewer amounts of yeast and are also restricted toward the bottom surface of the bigger holes. This is because, few effervescence centers are available from low yeast content which gives a few small pores. As a greater amount of yeast is made available, the extent of smaller pore formation expands toward a larger area (Figure 4a–e). The pore size and porosity are also found to increase with an increase in yeast volume. Large pore size arising from a higher density of effervescence centers increases porosity (Figure 4, parts f and g). Pore size increases 2-fold (~25 to ~55 μm) giving a nearly double increase in porosity as well (~35% to 60%). The standard deviation of these shows confined dispersion about their mean values emphasizing good repeatability and homogeneity of the approach. Thus, controlled and desired porosity can be achieved by controlling the volume of yeast solution added to the mixture which can be implemented for customized applications.

3.4. In-Situ Compression–Porosity Study. A tomography study shows the effect of compression on porosity and resilience of the sponge for long-term compression (Figure 5). A sponge of dimension $15 \times 15 \times 15 \text{ mm}^3$ was taken for this study and compressed in 5 steps of 2 mm each to a minimum height of 5 mm and was scanned with scan time ~4 h for each sponge height (Figure 5a). Images of the sponge in the middle plane were used to extract the porosity and pore size at each of the compressed state (Figure 5b). The pore volume decreases systematically (from ~65% at 15 mm height to ~23% at 5 mm height, Figure 5, parts c and d) with compression and is restored (to ~61%) after the applied load was removed. The postcompression scanning results showed that the pores were still intact, however, with some deformations with the porosity

reduced by ~4% after the load was removed. The high resilience can be attributed to the uniform dispersion of yeast and water in the PDMS by virtue of the surfactant that binds the PDMS and yeast solution throughout the volume of the mixture. The standard deviations of pore size and porosity show a narrow dispersion about their mean values validating the repeatability of the fabrication approach. The porous structure at each stage of compression is as a result of elastic buckling of the pore struts and final collapse at complete compression. This behavior is typical for an elastomer sponge, which is reflected in the PDMS sponge. The elastic buckling enables feature restoration upon release of applied load. The pore collapse leads to some deformation in the final structure after load is removed. Figure 5e shows the response of pores to different load applied condition.

3.5. Effect of Curing Temperature on Porosity and Sensitivity of Resistive Sensor. The hydrophilicity of the sponge was exploited to make the sponge resistive by a conductive ink (Figure S4 in the Supporting Information). A temperature-dependent study on the sensitivity of the resistive sensor was carried out by curing the mixture at 80, 100, 120, and 140 °C (Figure 6). The relative resistance change obtained for the different pressures applied over the sensor shows a linear increase until 30 kPa providing a large window of operation with good sensitivity of $\sim 0.3 \text{ kPa}^{-1}$ (Figure 6a). The pressure change with applied strain rises slowly until 80% strain after which it shoots up. Most of the resistance change thus occurs in the range up to ~100 kPa, which depicts that the whole volume of the sponge is operational in providing the obtained sensitivity window (Figure 6b). Furthermore, the pressure vs strain graph shows explicitly elastic buckling and densification alone occurring in the struts leading to elastic behavior of the sponge, giving a better resilience. The elastic buckling region defines the sensing obtained at lower applied

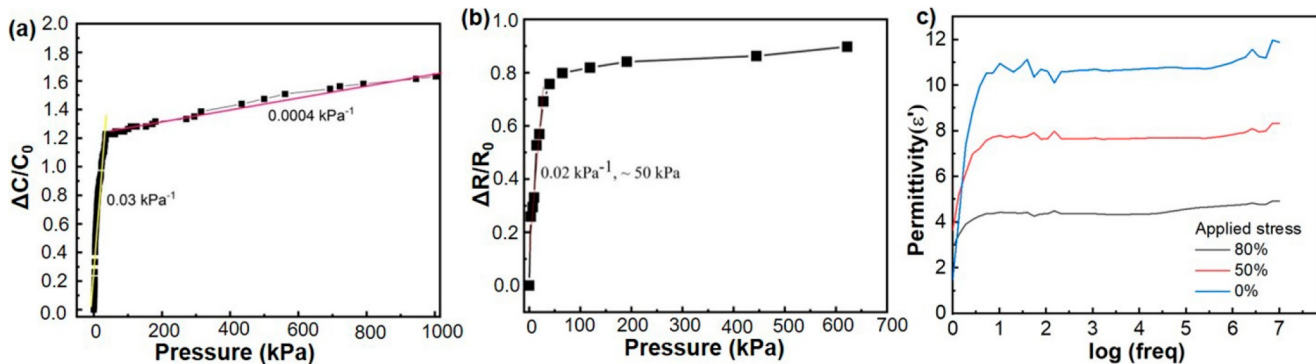


Figure 7. Extended sensing profile obtained by combining PDMS sponges obtained from different curing temperatures in (a) capacitive mode, (b) resistive mode, and (c) permittivity plotted for different compressed stages of the pristine hydrophilic sponge.

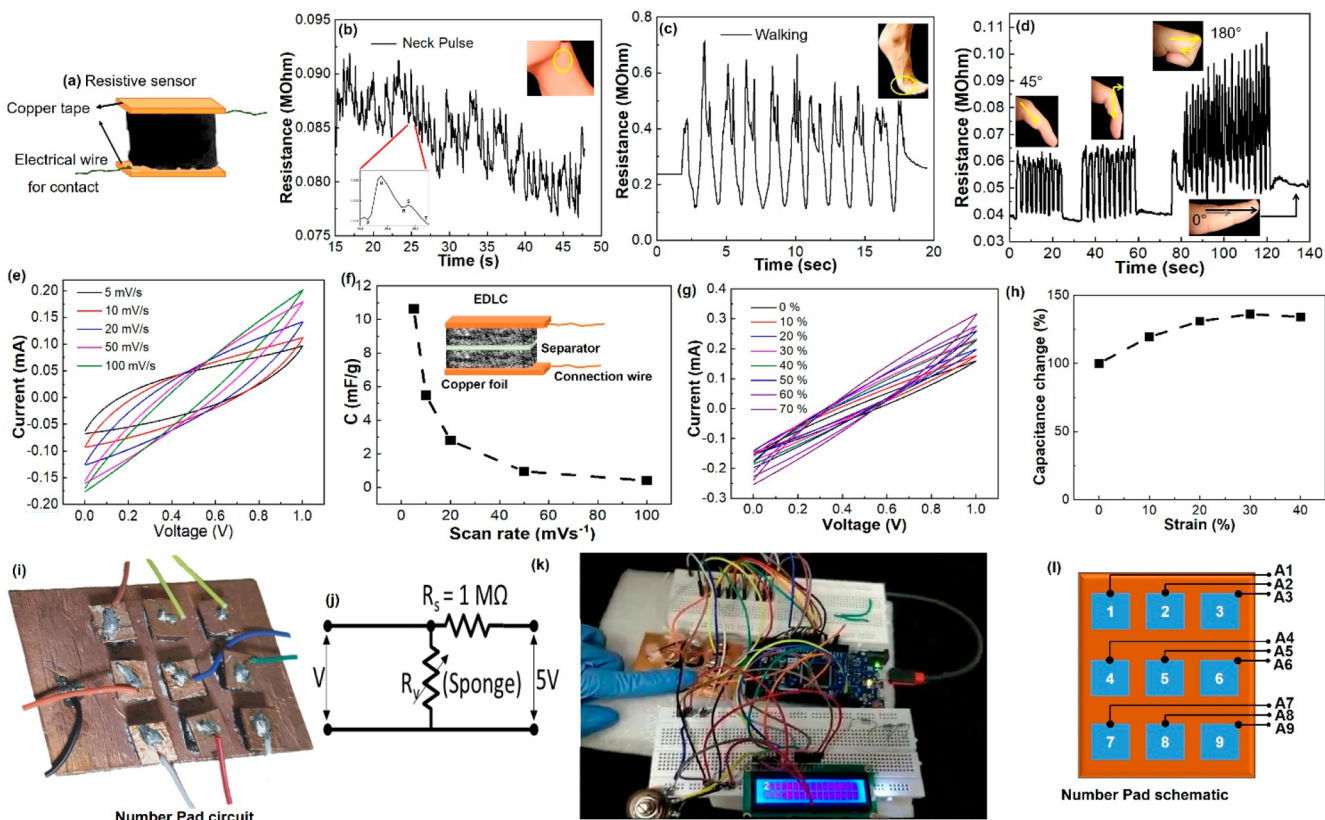


Figure 8. (a) Pressure sensor device schematic. (b) Neck pulse with inset showing the distinct peaks. (c) Plantar pressure of walking action. (d) Finger bend movements. Supercapacitor function of the porous electrode. (e) Scan rate varied response. (f) Gravimetric capacitance with device schematic in inset. (g) Capacitor response to applied stress. (h) Capacitance change to applied stress. (i) Human–machine interfacing with number pad circuitry. (j) Single pixel circuit equivalent. (k) Real time demonstration of number displayed and (l) Number pad outlay.

pressures, and densification gives sensing at higher pressures giving a wider range of pressure sensing. Also, the sensing range is confined to the elastic region from the stress–strain behavior which is ideal; however, complete exploitation of it has not been achieved as the sensitivity saturates at $\sim 10\%$ strain for 140 and 120 °C samples, and at $\sim 60\%$ strain for the 80 and 100 °C samples. Higher porosity provides better sensitivity as seen from Figure 6c. (Porosity calculations are carried out from the morphology images shown in Figure S1 in the Supporting Information.) Hence, an application-specific pressure sensor with a sensitivity of desired value in the desired operation window can be fabricated by the choice of its curing temperature.

These individual sponges provide good sensitivity at low-pressure range. The porosity varied fabrication and hence the change in sensitivity provides possibilities of implementing synergistic effect. This is achieved by using a sandwiched approach in device fabrication carried out here using sponges cured at 80 and 100 °C (Figure 7). Here, the device provides a sensitivity of 0.02 kPa^{-1} up to pressures $\sim 50 \text{ kPa}$. This ensures a complete sensing platform enabled from the porosity variation achieved from the curing of elastomer sponge. This extended range covers the entire physical sensing. Earlier sensors fabricated using elastomer sponges (Table S2 in the Supporting Information) depict a particular range alone needing separate sensor fabrication method for a different

pressure range. Owing to the better resilience of the PDMS sponge, its applicability to capacitive sensing was also checked to achieve extended sensing up to ~ 45 kPa with a sensitivity of ~ 0.03 kPa $^{-1}$ (Figure 7a).

A probe into the material aspect revealed a decrease in the dielectric permittivity with applied pressure, in contrast to an earlier report wherein an increase in permittivity was found with applied pressure.¹⁰ This behavior can be attributed to the weakening of the electric field within the material. As the sponge pores collapse, dipoles originating from the functional groups present in the pore strands cancel the net charge within the sponge volume, thus canceling the electric field strength in it. This thus contradicts and acts against the applied electric field which is encountered in sensing. This reduced electric permittivity leads to less change in capacitance giving less sensitivity to the capacitive device. We thus push here on its resistive sensor activity exploiting the hydrophilic nature and the resilience of the porous structure for varied applications. Our approach enables feasibility in achieving this with a simple single-step approach that can be applied to other applications showing its versatile nature as illustrated in section 3.6.

3.6. Versatile Applications of Resistive Sponge. The hydrophilic sponge is used in several possible applications showing the versatility achievable from the proposed single-step approach (Figure 8). The sensor device schematic has the resistive sponge as a sensing element with copper electrodes (Figure 8a). The flexible conformity of the sensor with skin enables precise sensing of arterial and plantar pressure. Neck pulse measurement with the inset showing the critical points on the curve corresponding to the heartbeat sequence are recorded (Figure 8b). The real-time forefoot contact with a floor surface during a walk sequence shows a typical walk sequence consisting of the heel, middle, and forefoot placement with proper impact gaining momentum for moving forward (Figure 8c). A proper foot profile is thus required for a healthy walk pattern, which can be affected by chronic diseases like diabetic patients tending to develop curved toes caused by insufficient blood circulation and nerve shrinkage. This leaves the toes numb with the loss of their natural sensing. A sensor for monitoring their progress in medication is thus necessary. This helps diagnose the extent of the impact of the chronic situation on the patient. The sensor is also used in tactile sensing of index finger motion for different angles from 45° to 180° (Figure 8d). All three periodic segments show repeatable and distinguishable responses. There is less enhancement in the sensing between 45° and 90°, which can be attributed to the lesser strain induced in the porous structures which does not perturb the conducting network in the sensor. However, at a 180° bent position, the sensor is considerably strained, providing perturbed conductivity increasing the resistance giving a distinct response from the 45° and 90° bent positions. Another versatile application for the proposed resistive sponge explored here is as a supercapacitor device. The resistive sponge forms electrodes with a glass microfiber filter as separator and copper foil as the current collector forming a symmetric supercapacitor. The device dimension of $10 \times 10 \times 10$ mm 3 gives equivalent volumetric and gravimetric capacitance values. The porosity provides a greater surface area to the carbon available for charge storage, giving supercapacitor functionality to the resistive sponge. The CV curves follow the trend for a supercapacitor with the area under the curve decreasing for higher scan rates (Figure 8e).

The scan rate is varied from 5 to 100 mV/s for a voltage window of 1 V. The CV curves show an ideal electrochemical double layer formation with the quasi rectangular and approximate symmetry about zero current giving a maximum capacitance of ~ 11.43 mF/g at 5 mV/s. The device is further studied under applied stress (Figure 8g) for its durability and robust nature which shows consistent and repeatable CV under applied stress of 0% to 40%. The stress-dependent performance of the capacitor device is shown in Figure 8h, where a small change in capacitance is observed with applied pressure for the porous structure of the sponge. These features of the supercapacitor add to the versatility of the proposed method of electrode fabrication. The human–machine interface capability of the sponge as a 3×3 sensor array is employed via a number pad (Figure 8i). Here, each sponge element or a pixel acts as a piezoresistive device, each pixel activity can be captured by measuring the voltage drop across it (Figure 8j). This algorithm can be used to control an actuator or electrical system. This whole setup with the real-time display is shown in Figure 8k, where an on press event of the resistive sponge corresponding to its number on the number pad is displayed on the LCD screen (see video in Supporting Information). This reliable application further paves way for human–machine interface systems with control possibilities which is an exciting venture.

4. CONCLUSION

A highly cost-effective and high yield single pot method of obtaining a hydrophilic PDMS sponge is detailed here wherein the porosity and pore size can be varied by varying the concentration of yeast, the volume of the yeast solution, and the curing temperature with a confined dispersive measure of standard deviation about the mean values of porosity and pore size, which confirms the homogeneity and repeatability. The morphology variations with porosity are studied with scanning electron microscopy imaging. The porosity increases with an increase in (i) concentration of yeast and (ii) volume of yeast solution as well as (iii) the curing temperature. A tomography study shows high resilience and sturdiness of the porous structures with negligible hysteresis in porosity arising from a little deformation in the porous structure after the 24 h long compression. The decrease in permittivity of the PDMS sponge qualifies it for resistive sensing applications. The sponge is thus made resistive using a dip-dry method in an electric paint. The obtained sponge is employed as a resistive sensor and is used for sensing tactile movement, low pulse pressures, and higher plantar pressures. These are also applied in human–machine interface systems with a real-time display of a number pad. A supercapacitor is also studied with the obtained resistive sponge as an electrode, which gives approximately ideal rectangular curves in the CV study. These varied applications provide a promising future to our approach of obtaining a hydrophilic elastomer sponge, which can be tuned as a resistive pressure sensor for a versatile pressure range.

ASSOCIATED CONTENT

SI Supporting Information

The Supporting Information is available free of charge at <https://pubs.acs.org/doi/10.1021/acsapm.1c00593>.

Additional studies on the variation of temperature (Figure S1), comparison of mechanical properties of

hydrophobic and hydrophilic PDMS sponges (Figure S2), capacitive sensor with extended pressure range sensing (Figure S3), resistive sensor fabrication (Figure S4), basic resistive sensor performance (Figure S5), sensing mechanism in stress and strain mode resistive sensing (Figure S6), additional real time sensing of index movement and pulse and plantar pressures (Figure S7) and internal circuit diagram of the number pad (Figure S8), comparison of the different sponge fabrication methods (Table S1), and existing resistive sensors are compared for their performance (Table S2) [PDF](#)

Video shows the operation of the number pad as a prototype for human-machine interfacing ([MP4](#))

AUTHOR INFORMATION

Corresponding Author

Dipti Gupta – Plastic Electronics and Energy Laboratory, Department of Metallurgical Engineering and Materials Science, Indian Institute of Technology Bombay, Mumbai 400076, India; [orcid.org/0000-0003-3252-3407](#); Email: diptig@iitb.ac.in

Authors

Chithra Parameswaran – Plastic Electronics and Energy Laboratory, Department of Metallurgical Engineering and Materials Science, Indian Institute of Technology Bombay, Mumbai 400076, India

Raghvendra Pratap Chaudhary – Department of Physics & Astronomy, Seoul National University, Gwanak-gu, Seoul KR 08826, South Korea

Sagar Hosangadi Prutvi – Plastic Electronics and Energy Laboratory, Department of Metallurgical Engineering and Materials Science, Indian Institute of Technology Bombay, Mumbai 400076, India; [orcid.org/0000-0002-0403-7842](#)

Complete contact information is available at:
<https://pubs.acs.org/10.1021/acsapm.1c00593>

Author Contributions

C.P. developed the approach and studied the material in detail. C.P. conducted all the experiments and confirmed their analysis. R.P.C. carried out the statistical calculations. C.P. carried out the sensing and super capacitor applications. S.H.P. designed the number pad circuit. The manuscript was proof read by C.P., R.P.C., S.H.P., and D.G.

Notes

The authors declare no competing financial interest.

ACKNOWLEDGMENTS

C.P. acknowledges funding received from the Department of Science and Technology (DST) as an INSPIRE fellowship (IF150332) and D.G. acknowledges funding received from DST as grants bearing Nos. DS.TSG/AMT/2015/617/G and DST/TMD/MES/2K17/93. The authors are thankful to SAIF, IIT Bombay, for characterization facilities of FTIR, SEM, and FDXM and the MEMS department for the SEM facility. The authors also acknowledge Prof. Amartya Mukhopadhyay (HTEM laboratory, MEMS, IIT Bombay), for facilitating measurements of supercapacitor performance.

REFERENCES

- (1) Cho, D.; Park, J.; Kim, J.; Kim, T.; Kim, J.; Park, I.; Jeon, S. Three-Dimensional Continuous Conductive Nanostructure for Highly Sensitive and Stretchable Strain Sensor. *ACS Appl. Mater. Interfaces* **2017**, *9*, 17369–17378.
- (2) Song, Y.; Chen, H.; Chen, X.; Wu, H.; Guo, H.; Cheng, X.; Meng, B.; Zhang, H. All-in-one piezoresistive-sensing patch integrated with micro-supercapacitor. *Nano Energy* **2018**, *53*, 189–197.
- (3) Yu, X.; Li, Y.; Zhu, W.; Huang, P.; Wang, T.; Hu, N.; Fu, S. A wearable strain sensor based on a carbonized nano-sponge/silicone composite for human motion detection. *Nanoscale* **2017**, *9*, 6680–6685.
- (4) Yao, H.; Ge, J.; Wang, C.; Wang, X.; Hu, W.; Zheng, Z.; Ni, Y.; Yu, S. A flexible and highly pressure-sensitive graphene-polyurethane sponge based on fractured microstructure design. *Adv. Mater.* **2013**, *25*, 6692–6698.
- (5) Han, J.; Kim, B.; Li, J.; Meyyappan, M. Flexible, compressible, hydrophobic, floatable, and conductive carbon nanotube-polymer sponge. *Appl. Phys. Lett.* **2013**, *102*, 051903.
- (6) Wu, X.; Han, Y.; Zhang, X.; Zhou, Z.; Lu, C. Large-Area Compliant, Low-Cost, and Versatile Pressure-Sensing Platform Based on Microcrack-Designed Carbon Black@Polyurethane Sponge for Human–Machine Interfacing. *Adv. Funct. Mater.* **2016**, *26*, 6246–6256.
- (7) Zhang, H.; Liu, N.; Shi, Y.; Liu, W.; Yue, Y.; Wang, S.; Ma, Y.; Wen, L.; Li, L.; Long, F.; Zou, Z.; Gao, Y. Piezoresistive Sensor with High Elasticity Based on 3D Hybrid Network of Sponge@CNTs@Ag NPs. *ACS Appl. Mater. Interfaces* **2016**, *8*, 22374–22381.
- (8) Wu, S.; Zhang, J.; Ladani, R. B.; Ravindran, A. R.; Mouritz, A. R.; Kinloch, A. J.; Wang, C. H. Novel Electrically Conductive Porous PDMS/Carbon Nanofiber Composites for Deformable Strain Sensors and Conductors. *ACS Appl. Mater. Interfaces* **2017**, *9*, 14207–14215.
- (9) Iglio, R.; Mariani, S.; Robbiano, V.; Strambini, L.; Barillaro, G. Flexible Polydimethylsiloxane Foams Decorated with Multiwalled Carbon Nanotubes Enable Unprecedented Detection of Ultralow Strain and Pressure Coupled with a Large Working Range. *ACS Appl. Mater. Interfaces* **2018**, *10*, 13877–13885.
- (10) Parameswaran, C.; Gupta, D. Low cost sponge based piezocapacitive sensors using a single step leavening agent mediated autolysis process. *J. Mater. Chem. C* **2018**, *6*, 5473–5481.
- (11) Choi, S.; Kwon, T.; Im, H.; Moon, D.; Baek, D. J.; Seol, M. L.; Duarte, J. P.; Choi, Y. K. A polydimethylsiloxane (PDMS) sponge for the selective absorption of oil from water. *ACS Appl. Mater. Interfaces* **2011**, *3*, 4552–4556.
- (12) Zhang, A.; Chen, M.; Du, C.; Guo, H.; Bai, H.; Li, L. Poly(dimethylsiloxane) Oil Absorbent with a Three-Dimensionally Interconnected Porous Structure and Swellable Skeleton. *ACS Appl. Mater. Interfaces* **2013**, *5*, 10201–10206.
- (13) Wang, X.; Lu, Y.; Carmalt, C. J.; Parkin, I. P.; Zhang, X. Multifunctional Porous and Magnetic Silicone with High Elasticity, Durability, and Oil–Water Separation Properties. *Langmuir* **2018**, *34*, 13305–13311.
- (14) Chavan, A.; Li, H.; Scarpellini, A.; Marras, S.; Manna, L.; Athanassiou, A.; Fragouli, D. Elastomeric Nanocomposite Foams for the Removal of Heavy Metal Ions from Water. *ACS Appl. Mater. Interfaces* **2015**, *7*, 14778–14784.
- (15) Song, Y.; Chen, H.; Su, Z.; Chen, X.; Miao, L.; Zhang, J.; Cheng, X.; Zhang, H. Highly Compressible Integrated Supercapacitor–Piezoresistance-Sensor System with CNT–PDMS Sponge for Health Monitoring. *Small* **2017**, *13*, 1702091.
- (16) Park, S.; Kim, H.; Vosgueritchian, M.; Cheon, S.; Kim, H.; Koo, J. H.; Kim, T. R.; Lee, S.; Schwartz, G.; Chang, H.; Bao, Z. Stretchable Energy-Harvesting Tactile Electronic Skin Capable of Differentiating Multiple Mechanical Stimuli Modes. *Adv. Mater.* **2014**, *26*, 7324–7332.
- (17) Li, X.; Li, Y.; Huang, Y.; Zhang, T.; Liu, Y.; Yang, B.; He, C.; Zhou, X.; Zhang, J. Organic sponge photocatalysis. *Green Chem.* **2017**, *19*, 2925–2930.

- (18) Zhou, T.; Yang, J.; Zhu, D.; Zheng, J.; Handschuh-Wang, S.; Zhou, X.; Zhang, J.; Liu, Y.; Liu, Z.; He, C.; Zhou, X. Hydrophilic Sponges for Leaf-Inspired Continuous Pumping of Liquids. *Adv. Sci.* **2017**, *4* (6), 1700028.
- (19) Cha, K. J.; Kim, D. S. A portable pressure pump for microfluidic lab-on-a-chip systems using a porous polydimethylsiloxane (PDMS) sponge. *Biomed. Microdevices* **2011**, *13*, 877–883.
- (20) Yang, W.; Nam, Y. G.; Lee, B. K.; Han, K.; Kwon, T. H.; Kim, D. S. Fabrication of a hydrophilic poly(dimethylsiloxane) microporous structure and its application to portable microfluidic pump. *Jpn. J. Appl. Phys.* **2010**, *49*, 06GM01.
- (21) Barvič, M.; Kliment, K.; Zavadil, M. Biologic properties and possible uses of polymer-like sponges. *J. Biomed. Mater. Res.* **1967**, *1*, 313–323.
- (22) Alonso, M. V.; Auad, M. L.; Nutt, S. R. Modeling the compressive properties of glass fiber reinforced epoxy foam using the analysis of variance approach. *Compos. Sci. Technol.* **2006**, *66*, 2126–2134.
- (23) Wang, L.; Yang, X.; Zhang, J.; Zhang, C.; He, L. The compressive properties of expandable microspheres/epoxy foams. *Compos. Part B Eng.* **2014**, *56*, 724–732.
- (24) Lim, Y.; Cha, M. C.; Chang, J. Y. Compressible and monolithic microporous polymer sponges prepared via one-pot synthesis. *Sci. Rep.* **2015**, *5*, 1–11.
- (25) Duan, G.; Jiang, S.; Moss, T.; Agarwal, S.; Greiner, A. Ultralight open cell polymer sponges with advanced properties by PPX CVD coating. *Polym. Chem.* **2016**, *7*, 2759–2764.
- (26) Mooney, D. J. Tissue engineering with biodegradable polymer matrices. *IEEE Proc. 1996 Fifteenth South. Biomed. Eng. Conf.* **1996**, 537–540.
- (27) Mooney, D. J.; Baldwin, D. F.; Suh, N. P.; Vacanti, J. P.; Langer, R. Novel approach to fabricate porous sponges of poly (D, L-lactic-co-glycolic acid) without the use of organic solvents. *Biomaterials* **1996**, *17*, 1417–1422.
- (28) Mader, M.; Jérôme, V.; Freitag, R.; Agarwal, S.; Greiner, A. Ultraporous, Compressible, Wettable Polylactide/Polyacaprolactone Sponges for Tissue Engineering. *Biomacromolecules* **2018**, *19*, 1663–1673.
- (29) Zhu, D.; Handschuh-Wang, S.; Zhou, X. Recent progress in fabrication and application of polydimethylsiloxane sponges. *J. Mater. Chem. A* **2017**, *5*, 16467–16497.
- (30) Park, J.; Wang, S.; Li, M.; Ahn, C.; Hyun, J. K.; Kim, D. S.; Kim, D. K.; Rogers, J. A.; Huang, Y.; Jeon, S. Three-dimensional nanonetworks for giant stretchability in dielectrics and conductors. *Nat. Commun.* **2012**, *3*, 916.
- (31) Fritz, J. L.; Owen, M. J. Hydrophobic recovery of plasma-treated polydimethylsiloxane. *J. Adhes.* **1995**, *54*, 33–45.
- (32) Zargar, R.; Nourmohammadi, J.; Amoabediny, G. Preparation, characterization, and silanization of 3D microporous PDMS structure with properly sized pores for endothelial cell culture. *Biotechnol. Appl. Biochem.* **2016**, *63*, 190–199.
- (33) Kim, H. T.; Kim, J. K.; Jeong, O. C. Hydrophilicity of surfactant-added poly(dimethylsiloxane) and its applications. *Jpn. J. Appl. Phys.* **2011**, *50*, 06GL04.
- (34) Fan, Y.; Meng, X. S.; Li, H. Y.; Kuang, S. Y.; Zhang, L.; Wu, Y.; Wang, Z. L.; Zhu, G. Stretchable Porous Carbon Nanotube-Elastomer Hybrid Nanocomposite for Harvesting Mechanical Energy. *Adv. Mater.* **2017**, *29*, 1603115.
- (35) Noh, J. S. Conductive elastomers for stretchable electronics, sensors and energy harvesters. *Polymers (Basel)* **2016**, *8*, 123.
- (36) Vosti, D. C.; Joslyn, M. A. Autolysis of Baker's Yeast. *Appl. Microbiol.* **1954**, *2*, 70–78.
- (37) Manners, B. D. J.; Masson, A. J.; Patterson, J. C. The Structure of a P- (1→ 3) -D-Glucan from Yeast Cell Walls. *Biochem. J.* **1973**, *135*, 19–30.
- (38) Lipke, P. N.; Ovalle, R. Cell Wall Architecture in Yeast : New Structure and New Challenges. *J. Bacteriol.* **1998**, *180*, 3735–3740.
- (39) Vernon, P. S.; Rose, A. H. Adsorption of Silicone Antifoam by *Saccharomyces Cerevisiae*. *J. Inst. Brew.* **1976**, *82*, 336–340.
- (40) Park, J.; Wang, S.; Li, M.; Ahn, C.; Hyun, J. K.; Kim, D. S.; Kim, D. K.; Rogers, J. A.; Huang, Y.; Jeon, S. Three-dimensional nanonetworks for giant stretchability in dielectrics and conductors. *Nat. Commun.* **2012**, *3*, 916.
- (41) Vickers, J. A.; Caulum, M. M.; Henry, C. S. Generation of hydrophilic poly(dimethylsiloxane) for high-performance microchip electrophoresis. *Anal. Chem.* **2006**, *78*, 7446–7452.
- (42) Drelich, J.; Chibowski, E.; Meng, D. D.; Terpilowski, K. Hydrophilic and superhydrophilic surfaces and materials. *Soft Matter* **2011**, *7*, 9804–9828.
- (43) Cai, D.; Neyer, A.; Kuckuk, R.; Heise, H. M. Raman, mid-infrared, near-infrared and ultraviolet – visible spectroscopy of PDMS silicone rubber for characterization of polymer optical waveguide materials. *J. Mol. Struct.* **2010**, *976*, 274–281.
- (44) Zimkus, A.; Misiunas, A.; Chaustova, L. Spectroscopic study of yeast *Saccharomyces cerevisiae* cell wall structure. *Chemija* **2011**, *22*, 80–84.
- (45) Bokobza, L.; Buffeteau, T.; Desbat, B. Mid- and Near-Infrared Investigation of Molecular Orientation in Elastomeric Networks. *Appl. Spectrosc.* **2000**, *54*, 360–365.
- (46) Burattini, E.; Cavagna, M.; Dell'Anna, R.; Malvezzi Campeggi, F.; Monti, F.; Rossi, F.; Torriani, S. A. FTIR microspectroscopy study of autolysis in cells of the wine yeast *Saccharomyces cerevisiae*. *Vib. Spectrosc.* **2008**, *47*, 139–147.

□ Recommended by ACS

Directional Self-Transportation of Droplets on Superwetting Wedge-Shaped Surface in Air and Underliquid Environments

Peizhang Zhou, Cailong Zhou, et al.

FEBRUARY 05, 2023

ACS APPLIED MATERIALS & INTERFACES

READ ▶

Robust Superhydrophobic PDMS@SiO₂@UiO66-OSiR Sponge for Efficient Water-in-Oil Emulsion Separation

Guanzhong Zhai, Daohua Sun, et al.

MARCH 24, 2023

INORGANIC CHEMISTRY

READ ▶

Controlling Superhydrophobicity and Oleophobicity of Polydimethylsiloxane-Coated Silica Hybrid Particles

Chan Beom Park, Jun Hyup Lee, et al.

MARCH 22, 2023

LANGMUIR

READ ▶

Solvent Volatilization-Induced Cross-Linking of PDMS Coatings for Large-Scale Deicing Applications

Yadong Yu, Jiadao Wang, et al.

DECEMBER 12, 2022

ACS APPLIED POLYMER MATERIALS

READ ▶

Get More Suggestions >